Sociedad Mexicana de Ingeniería Mecánica
Fecha de recepción: 02-09-2013
Fecha de aceptación: 15-01-2014

INGENIERÍA MECÁNICA
TECNOLOGÍA Y DESARROLLO
Vol. 4 No. 6 (2014) 219 - 228

Solution of the Inverse Bio-Heat Transfer Problem for a Simplified Dermatological Application: Case of Skin Cancer

[1]José Manuel Luna, [2]Abel Hernández Guerrero, [3]Ricardo Romero Méndez, [4]José Luis Luviano Ortiz

[1] Instituto Tecnológico Sanmiguelense de Estudios Superiores
[2]Universidad de Guanajuato
[3]Universidad Autónoma de San Luis Potosí
[4]Universidad Nacional Autónoma de México

Resumen

En esta investigación se ha implementado una técnica numérica fundamentada en el acoplamiento del método de elementos de frontera con la técnica de templado simulado, con la finalidad de resolver el problema inverso de transferencia de calor para una aplicación dermatológica. La minimización de la función objetivo se ha dirigido hacia la posibilidad de estimar parámetros termo-físicos y geométricos de tumores hipotéticos muy pequeños alojados en el tejido de la piel (tumores con niveles de profundidad < 3 mm). La investigación considera que el proceso de transferencia de calor en los tejidos de la piel y el tumor puede describirse por el modelo de bio-transferencia de Pennes bajo la consideración de metabolismo y perfusión sanguínea homogéneos, previo a la etapa de necrosis por parte del tumor. Debido a la falta de información experimental, la solución del problema inverso se ha llevado a cabo utilizando campos superficiales de temperatura contaminados con diferentes niveles de ruido con el fin de simular la distribución de temperatura que se obtendría in-situ por un equipo termográfico durante una prueba clínica. La convergencia hacia los valores esperados ha mostrado la generalidad de la técnica en diferentes casos de estudio.

Abstract

In this investigation, a numerical procedure, based on the Boundary Element Method coupled with the Simulated Annealing technique, has been used for estimating thermo-physical and geometrical parameters of very small hypothetical skin tumors using a surface temperature profile. For this, it was assumed that the thermo-physics of the yet-to-be detected cancerous lesion is described by Pennes' model with homogeneous perfusion and metabolism before necrosis. Several results are presented for tumors of Clark levels II–IV to illustrate the generality of the methodology. Different levels of noise have been imposed in the temperature fields obtained in the direct problem in order to simulate the input experimental temperature fields. The bio-heat transfer model has been solved in steady state simulating a state of extremely rest, which is the condition of a patient during a clinical trial.

Palabras clave:
Método de elementos de frontera, templado simulado, bio-transferencia de calor, problema inverso de transferencia de calor, cáncer de piel.

Keywords:
Boundary element method, simulated annealing, inverse heat transfer problem, bio-heat transfer, skin cancer.

Nomenclature

A	Matrix containing the coefficients of the linear system of equations.
B	Column vector of the linear system of equations
c	Specific heat of tissue.
c_1, c_2	Constants.
d	Tumor thickness.
d^*	Perturbed valued for d.
E	Objective function.
G, H	Matrices with influence coefficients.
h	Convective heat transfer coefficient.
K	Constant in the Metropolis' criterion.
k	Thermal conductivity of tissue.
l	Length domain.
m_b	Blood mass flow rate.
N	Number of annealing temperatures.
n	Unit normal vector.
P_a	Probability of acceptance.
Q_{met}	Metabolic heat generation.
q	Column vector containing normal derivatives.
rand	Random value in the range 0-1.
r, z	Cylindrical coordinates.
S	Secondary matrix.
T	Column vector containing boundary temperatures.
T_a	Arterial temperature.
T_c	Core body temperature.
T	Tissue temperature.
T^*	Dimensionless temperature.
T_{ann}	Annealing temperature.

T_{exact}	Exact temperature.
T_{∞}	Ambient temperature.
t	Time.
$\mathbf{T}_{comp}$	Vector containing computed temperatures.
$\dot{V}_{o_2}$	Oxygen consumption of tissue.
w	Tumor width.
$\mathbf{X}$	Vector containing the unknown tumor parameters.
$\mathbf{x}$	Column vector containing unknowns of the linear system.
$\mathbf{Y}$	Vector containing measured temperatures.

Greek symbols

Γ_1	Outer boundary.
$\Gamma_{1,2}$	Interface between Ω_1 and Ω_2.
ε	Random value.
λ	Mass fraction.
ρ	Density of tissue.
σ	Standard deviation of noise.
Ω_1, Ω_2	Computational domains.
ω_b	Blood perfusion rate.
ω_b^*	Perturbed value for ω_b.

Introduction

According to the Mexican Department of Health, since 2001 skin cancer has been the second type of cancer diagnosed in Mexico. Malignant melanoma is the most fatal type of skin cancer because it is originated in the melanocytes, the cells which produce the pigment melanin that colors our skin, hair, and eyes. According to Riegel et al. [1], in the 1930s the risk of a person developing malignant melanoma was 1 in 1500 worldwide. At the current rate, that risk is 1 in 74. According to Clark et al. [2] and Breslow [3], the survival prognosis in melanoma is directly proportional to the invasion level of the tumor as deeper melanomas metastasize more easily as they can reach the subcutaneous blood vessels. Therefore, maximum tumor thickness is the most important prognostic factor for patients with primary cutaneous melanoma. The five-year survival rate for patients with early melanoma, defined as thinner than 1 mm, is 94% versus less than 50% for those with melanomas greater than 3 mm thick. Therefore, early accurate diagnosis is crucial for a successful clinical treatment. Although a biopsy followed by a histopathological examination is the standard methodology for diagnosis, this cancer has the potential of being diagnosed through noninvasive techniques because of its cutaneous location. Among various types of noninvasive medical techniques for cancer detection, such as ultrasound or magnetic resonance imaging, thermal methods appear to be reliable, safe and mainly nonexpensive. Since the discovery by Warburg [4] of the glycolytic metabolism of malignant tumors, it has widely been demonstrated that they behave differently than healthy tissue in terms of heat production and dissipation. Therefore, since 1964 (Brasfield et al. [5]), infrared thermography (IR) has been used as an alternative method to detect cancer based on the abnormal temperature that result at the skin surface by the presence of the tumor. Recently, Cetingul and Herman [6] performed an experimental study to verify the feasibility of IR in distinguishing benign from malignant skin cancerous lesions. 35 patients with skin pigmented lesions were studied and only two of these cases were found to be malignant melanoma. The clinical assessment of these lesions was done by checking the ABCDE criteria for melanoma identification prior to biopsy. Similar investigations have concluded that IR is a promising method for detecting cutaneous and subcutaneous cancerous lesions (Santa Cruz et al. [7] and Keyserlingk [8]). Nevertheless, this technique needs to explore the relationship between the abnormal skin surface temperature and the characteristics of the cancerous lesion (tumor thickness and blood perfusion) to become a simple, quantitative, objective, and noninvasive in situ screening and diagnostic tool to evaluate the cancerous lesions. In order to complement the IR imaging technique, several methodologies based on the solution of the inverse bio-heat transfer problem have been proposed in order to estimate thermo-physical and geometrical tumor parameters. For example, Paruch and Majchrzak [9] estimated thermo-physical parameters of hypothetical tumors using a least-square algorithm based on sensitivity coefficients. In some cases of study, the algorithm developed was not always convergent or a wrong solution was obtained. Partridge and Wrobel [10], as well as Mital and Scott [11], used a genetic algorithm to estimate the position and size of hypothetical embedded tumors from surface temperature fields. The code developed was not capable of obtaining a solution for the case of very small and deep simulated tumors. The inverse problem was also solved by Agnelli et al. [12] using a second order finite difference scheme coupled with the pattern search algorithm. Even in the case when 5% and 10% of noise was added to the input data, the methodology estimated different parameters with very good accuracy. However, experiments for the case of very small and deep tumors were not performed. In order to contribute to the field of the inverse estimation process, Luna et al. [13] have developed a new methodology based on the boundary element method coupled to simulated annealing. Results of this investigation show a better quality in the parameter estimates compared to those obtained by other authors. However, this technique has not been tested if the variation in the surface temperature field caused by the hypothetical tumor is extremely small. Therefore, in order to demonstrate the robustness of the technique, it has been adapted to the special case of skin cancer, for which it has been demonstrated that it leads to a very small surface temperature gradient at very early growth stages [6]. In this case, the simultaneous estimation of the hypothetical skin tumor thickness and blood perfusion rate is carried out by considering the thermo-physical information available in the literature for skin and malignant melanoma, as well as the sizes defined by the Clark levels of invasion [2].

Modeling of Skin and Tumor Tissues

Malignant melanoma is characterized by uncontrolled growth of melanocytes, which are at the base of the epidermis, leading to irregular tumor shapes. In order to quantify the differences between the thermal responses of irregular and regular (symmetrical) tumor shapes, Cetingul and Herman [14] compared the responses of irregular 3D tumors with very small symmetrical tumors, as well as with a cylindrical region that has the same cross-sectional area. A negligible temperature difference in the surface temperature profile was found. Based on this result, the analysis in this work was carried out considering a 2D domain considering that the tumor is embedded into the skin about 0.1 mm below the surface, as shown in Figure 1. Similar to the assumptions taken by Liu and Xu [15], the skin region was considered as a unified tissue.

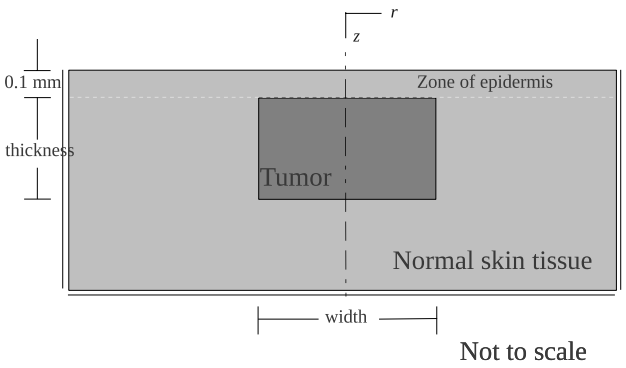

Figure 1. Representation of a malignant melanoma tumor embedded in the skin tissue.

The level of invasion, or tumor thickness, is the depth of a melanoma lesion measured from the base of the epidermis to the deepest identified melanoma tumor cells. This work considers primary melanomas, which are characterized by less than 2 mm invasion and without necrosis. Different Clark levels of invasion and tumor widths were considered in the study, as listed in Table 1.

Thermal Properties. In this work the density, heat capacity and thermal conductivity of the skin were calculated using the correlations developed by Cooper and Trezek [16]. Values of density, heat capacity and conductivity for the tumor were assumed to be similar to the properties of water due to lack of information. On the other hand, based on experiments by Stucker et al. [17] and experimental data compilation by Vaupel et al. [18], the blood perfusion of malignant melanoma is considered to be from three to eight times larger than in normal skin tissue.

Table 1. Dimensions of the tumors considered in the study.

Clark level	Level II	Level III	Level IV
Width (mm)	0.5 – 1.0	0.8 – 1.5	1.0 – 2.0
Thickness (mm)	0.5 – 0.75	0.8 – 1.0	1.5 – 2.0

Table 2. Values of the thermo-physical properties used in the study.

Tissue	c (J/kg.°C)	k (W/m.°C)	ρ (kg/m³)	ω_b ($ml_b/s.ml_t$)	Q_{met} (W/m³)
Skin	--	0.53	--	0.00085[a]	368
Tumor	--	0.558[b]	1030[b]	0.0026 to 0.0047	3072 to 6016
Blood	3770[d]	--	1060[c]	--	--

[a]Vaupel et al. [18]
[b]Cetingul and Herman [14]
[c]Duck [22]
[d]Torvi and Dale [23]

According to Huckaba et al. [19], the total metabolic heat production of the human body at rest is uniformly distributed between the skin (1.96%) and the body (98.04%). The metabolic rate of a neoplastic tissue, however, is independent of the total metabolic value and is directly related to the mass, perfusion rate, and oxygen consumption of the neoplastic tissue. Therefore, in this work the rate of oxygen consumption of the tumor has been obtained by using the values given for the blood perfusion (ω_b, $ml_b/s.ml_t$) previously transformed to blood flow units (m_b, ml/g.min) by using volume and time conversion factors, as well as the tumor density. Thus, Equation (4), which was proposed by Kallinowsky et al. [20] for different types of human tumors, including malignant melanoma, is evaluated to obtain the corresponding oxygen consumption ($\dot{V}_{O_2}$, μl/g.min). If it is assumed that 2×10^3 J of heat are liberated per liter of oxygen used, according to Sien and Jain [21], the oxygen consumption is multiplied by the above heat value to obtain the heat produced by the tumor. This value is then used during the evaluation of the bio-heat model. The complete set of parameter values used in the analysis is listed in Table 2.

$$V_{O_2} = 34.3m_b + 3.8 \tag{4}$$

Mathematical Model. The mathematical relationship given by Equation (5) was used to model the bio-heat transfer in both healthy and cancerous tissue by assuming steady state conditions in order to simulate the real situation during a clinical trial.

$$\nabla \bullet k\nabla T + \omega_b \rho_b c_b \left(T_a - T\right) + Q_{met} = 0 \tag{5}$$

In this model, developed by Pennes in 1948 [24], the blood perfusion is considered as a uniform heat sink/source term; the model neglects the direction of local capillary perfusion, and the influence of larger vessels in proximity to the local tissue. Shih et al. [25] present a detailed summary of the formulation of nine different bio-heat equations, including, among others, Mitchell and Myers' model, Keller and Seiler' model, and Chen and Holmes´ model, for which the main contribution is the effect of the countercurrent flow between vein and capillary blood flow.

If constant properties and steady state conditions are assumed, Equation (5) can be rewritten as:

$$\nabla^2 T = c_1 T - c_2 \tag{6}$$

where $c_1=\omega_b\rho_b c_b/k$ and $c_2=(\omega_b\rho_b c_b T_a+Q_{met})/k$. This equation is solved using the DRBEM, method in which the fundamental solution of Laplace's equation is used to approximate the term on the left-hand side. On the other hand, the nonhomogeneous part, $b=c_1T-c_2$, is approximated as a linear combination of interpolation functions expressed in matrix form as $\mathbf{b}=\mathbf{F}\boldsymbol{\alpha}$, where $\boldsymbol{\alpha}$ is a vector containing the nodal values of unknown coefficients. By applying both approximations, this leads to the system of equations given by: $\mathbf{HT}-\mathbf{Gq}=(\mathbf{H}\hat{\mathbf{U}}-\mathbf{G}\hat{\mathbf{Q}})\mathbf{F}^{-1}\mathbf{b}$

where the matrix **F** is calculated once the interpolation function has been defined. Letting $\mathbf{S}=(\mathbf{H}\hat{\mathbf{U}}-\mathbf{G}\hat{\mathbf{Q}})\mathbf{F}^{-1}$ this system of equations can be rewritten as in Equation (7). This equation will be used to model the skin cancer bio-heat transfer by taking into account the computational domain shown in Figure 2, which consists of two subdomains, Ω_1 and Ω_2, representing the healthy skin and tumor, respectively. Explicit details for the deduction of Equation (7) can be revised in [13]; therefore the symbols have their usual meaning.

$$(\mathbf{H}-c_1\mathbf{S})\mathbf{T}-\mathbf{Gq}=c_2\mathbf{S} \tag{7}$$

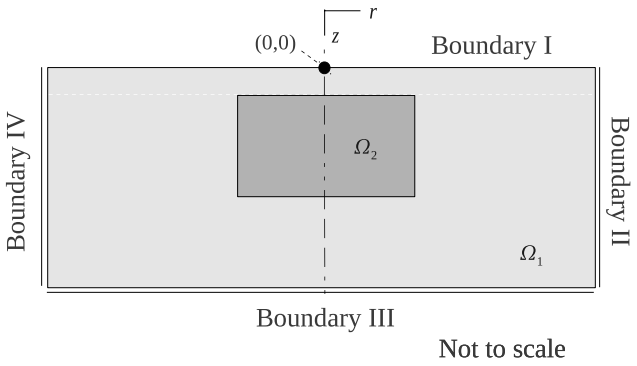

Figure 2. Computational domain.

As this potential problem is a composite domain problem, it should be solved by applying Equation (7) separately for each subdomain. The reason for this is that the fundamental solution is valid only for homogeneous domains. Therefore, applying this equation to the composite domain of Figure 2, the following systems of equations are obtained:

- for the healthy skin (Ω_1)

$$(\mathbf{H}-c_1\mathbf{S})^{\Omega_1}_{\Gamma_1}(\mathbf{H}-c_1\mathbf{S})^{\Omega_1}_{\Gamma_{1,2}}\begin{Bmatrix}\mathbf{T}^{\Omega_1}_{\Gamma_1}\\ \mathbf{T}^{\Omega_1}_{\Gamma_{1,2}}\end{Bmatrix}-\left[\mathbf{G}^{\Omega_1}_{\Gamma_1}\mathbf{G}^{\Omega_1}_{\Gamma_{1,2}}\right]\begin{Bmatrix}\mathbf{q}^{\Omega_1}_{\Gamma_1}\\ \mathbf{q}^{\Omega_1}_{\Gamma_{1,2}}\end{Bmatrix}=c_2\mathbf{S}^{\Omega_1} \tag{8}$$

- for the tumor (Ω_2)

$$(\mathbf{H}-c_1\mathbf{S})^{\Omega_2}_{\Gamma_{1,2}}\left\{\mathbf{T}^{\Omega_2}_{\Gamma_{1,2}}\right\}-\left[\mathbf{G}^{\Omega_2}_{\Gamma_{1,2}}\right]\left\{\mathbf{q}^{\Omega_2}_{\Gamma_{1,2}}\right\}=c_2\mathbf{S}^{\Omega_2} \tag{9}$$

Equations (8) and (9) are solved by imposing appropriate boundary conditions and continuity equations for the temperature and heat flux at the interface between healthy tissue and tumor ($\Gamma_{1,2}$). Once the continuity equation, given by Equations (10) where $\mathbf{k}_{1,2}$ is the square conductivity matrix, and boundary conditions are applied, the problem is combined into the single system of equations which is solved by the Gauss elimination scheme.

$$\begin{cases}\mathbf{T}^{\Omega_1}_{\Gamma_{1,2}}=\mathbf{T}^{\Omega_2}_{\Gamma_{1,2}}\\ \mathbf{q}^{\Omega_2}_{\Gamma_{1,2}}=-\mathbf{k}_{1,2}\mathbf{q}^{\Omega_1}_{\Gamma_{1,2}}\end{cases} \tag{10}$$

The present study considers small cancerous lesions and a larger area of healthy tissue surrounding the lesion. Both domains are modeled as a homogeneous tissue and the model that represents the skin tissue is considered to be large enough in order to consider negligible thermal effects of the tumor at the boundaries r=-6 mm, r=6 mm, and z=10 mm. The skin surface, Boundary I in Figure 3, is exposed to the natural convective condition at ambient air temperature (T_∞=25°C, h=10 W/m^2.°C). The bottom surface is assumed to be at core temperature ($T=T_c$=37°C). The exterior boundary was discretized with 120 linear elements and multiple nodes were used at the corners to take into account the discontinuity of the boundary conditions, as shown in Figure 3. Each edge of the interface was divided into 30 linear elements as well.

One concern in the present study is which kind of tumors can be detected through only the surface temperature, as well as the tumor parameters that can be detected. This is in fact restricted by the sensitivity of the surface thermometry and the algorithm applied, and more importantly, by the understanding of the tumor physiology. Before performing the inverse analysis, the DRBEM has been implemented for solving the steady state direct problem defined by Equation (5) by considering the tumor sizes listed in Table 1, as well as the range for the tumor blood perfusion rate given in Table 2, and the boundary conditions previously defined. Results of this sensitive analysis are presented in Figures 4 and 5, respectively.

By considering a constant value for the blood perfusion rate (0.0047 ml$_b$/s.ml$_t$), Figure 4 shows the skin surface temperature distribution for tumors with several Clark levels of invasion. Note that $T_{healthy}$ is the surface temperature of a region far away from the tumor, ΔT_{max} is the maximum temperature difference obtained for all the cases studied, and l=12 mm is the length of the skin tissue.

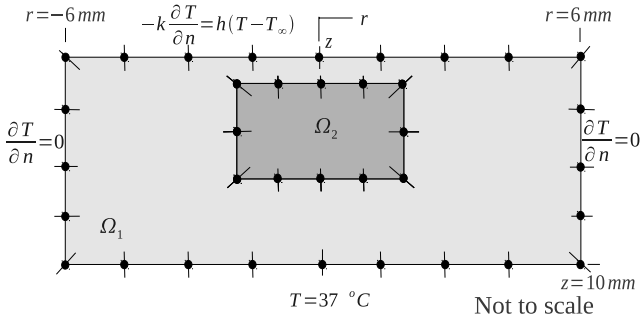

Figure 3. Boundary conditions used for application of the DRBEM.

Noting that the temperature is symmetric since the tumor is centered at r=0 , the profiles indicate that the surface temperature distributions are sensitive to the tumor size as this

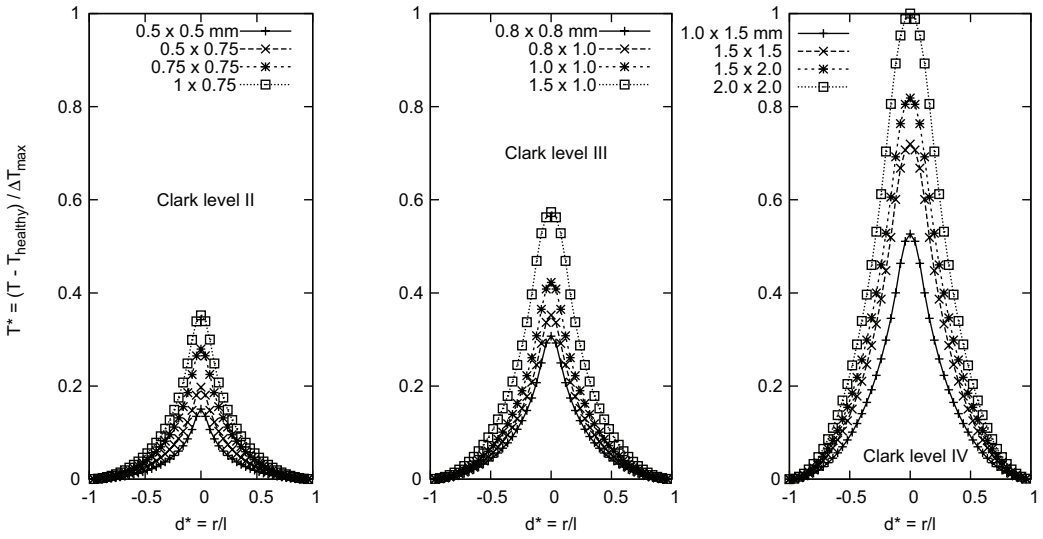

Figure 4. Effect of the tumor size on the surface temperature distribution.

parameter affects both the peak temperature (the temperature just above the neoplasm) and the shape of the profile. As expected, the surface temperature difference increases as the tumor size is increased. Therefore, it is possible to obtain inversely an estimate of the invasion level by using the surface temperature, and this can be used to attempt to stage melanoma lesion during a clinical evaluation. The thermal response of a tumor with different blood perfusion rates was also investigated. Figure 5 shows the computed dimensionless skin surface temperatures over a tumor of Clark level IV for a range of ω_b values, and assuming constant tumor size ($w \times d$=2 ×2 mm). The results indicate that the surface temperature distributions are sensitive to the tumor blood perfusion as well. As expected, the temperature difference increases as the blood perfusion is increased. This suggests that it might be easier to detect tumors with high blood perfusion rates.

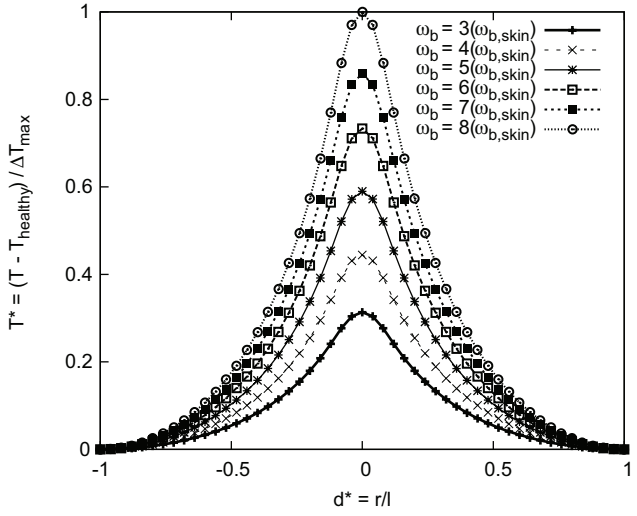

Figure 5. Effect of the tumor blood perfusion on the surface temperature distribution.

Estimation Methodology

Objective Function. This work is concerned with the simultaneous estimation of the skin tumor blood perfusion rate and the thickness of the tumor using the skin surface temperature distribution. The solution of this inverse problem is based on the minimization of the value of the sum of the squares of the differences between the temperatures measured at nodes on the skin surface and the computed temperature obtained from the solution of the direct problem with estimates for the unknown quantities by using the DRBEM. This objective function (E) is defined by Equation (15), where **Y** and **T** are vectors containing the measured and estimated temperatures, respectively, and the superscript *T* denotes the transpose of the vector. Let $\mathbf{X}=[d \quad \omega_b]$ be the set of unknown tumor parameters.

$$E = \left(\mathbf{Y} - \mathbf{T}(\mathbf{X})\right)^T \left(\mathbf{Y} - \mathbf{T}(\mathbf{X})\right) \tag{15}$$

Measured Temperature Data. In the most up-to-date technical literature it has been found that the technological advances in thermo-graphical cameras allow temperature measurements with less than 1% deviation error, and thermal resolution (minimum temperature difference) of less than 14 mK. On the other hand, according to Fogelson et al. [26], the error associated to thermocouples used for measuring human body temperature is 0.05 °C. Based on this information, noise with different levels of standard deviations (σ) was inserted in the surface temperature distributions obtained in the direct solution, as shown in Figure 7, to simulate the experimental temperature fields used as input data in the inverse process due to lack of experimental information. Such noise was imposed as: $Y=T_{exa}+\varepsilon$, where T_{exa} is the exact local temperature, taken from Figures 5 and 6, and ε is a random value taken from the range ±0.05 °C. Although these errors do not seem significant, the surface temperature differences are so small and the effect of these levels of noise perturbs significantly the curve of the exact solution, as shown in Figure 6.

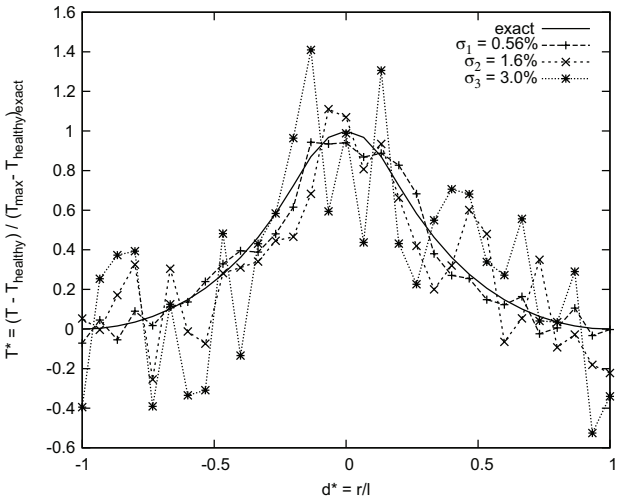

Figure 6. Perturbed surface temperature used as measured temperature data.

Minimization Technique. The technique of simulated annealing is basically a process of three steps: perturb, evaluate, and accept the solution if it is better than a solution previously chosen [27]. At the beginning, before any perturbation, the initial solution ($\mathbf{X}_0$) is created by assigning random values for the tumor thickness and for the blood perfusion rate from the ranges given by Equation (16).

$$\begin{aligned} 0.1 \le d \le 3.0 \quad & \text{mm} \\ 0.00085 \le \omega_b \le 0.0085 \quad & \text{ml}_\text{b}/\text{s.ml}_\text{t} \end{aligned} \tag{16}$$

This work considers the temperature-dependent perturbation scheme given by Equation (17), in which the value of each parameter is added to a random value whose maximum amplitude is proportional to the current annealing temperature.

$$\begin{aligned} d^* &= d + \left(2 \times T_{ann} \times rand\right) - T_{ann} \quad \text{mm} \\ \omega_b^* &= \omega_b + \left(2 \times T_{ann} \times rand\right) - T_{ann} \quad \text{ml}_\text{b}/\text{s.ml}_\text{t} \end{aligned} \tag{17}$$

where *rand* is a random value between 0 and 1. The number of iterations per annealing temperature has been chosen between 10 and 50 based on the available computing resources. The acceptance criterion is to accept a solution whenever it has an error lower than that of the previous solution. The *Metropolis Algorithm* [28], defined by Equation (18), follows this criterion and was used to compute the probability of acceptance (P_a) for a perturbed solution.

$$P_a = \begin{cases} 1 & \Delta E < 0 \\ \exp\left(-\dfrac{K\Delta E}{T_{ann}}\right) & \Delta E > 0 \end{cases} \tag{18}$$

where $\Delta E = E_{i+1} - E_i = E(\mathbf{X}_{i+1}) - E(\mathbf{X}_i)$ is the difference between the solution after it has been perturbed and the current solution. In order to reduce the time spent on vain perturbations, the method given by Ledesma et al. [29] was considered in this work for estimating the value of K. The way in which the annealing temperature decreases was set by following the exponential schedule given by Equation (19).

$$\begin{aligned} T_{ann,i} &= T_{ann,0} \exp\left(-Ai\right) \\ A &= \left(\frac{1}{N}\right) \ln\left(\frac{T_{ann,0}}{T_{ann,\text{i}}}\right) \end{aligned} \tag{19}$$

where $T_{ann,i}$ represents the i-th annealing temperature, being $T_{ann,0}$ and $T_{ann,\text{N}}$ the initial and final annealing temperatures, respectively. Before the beginning of annealing, the initial annealing temperature is taken as the average value of the objective function evaluated at ten randomly selected points in the space defined by Equation (16). In addition, the annealing temperature is allowed to decrease until it reaches a very small value close to zero. Therefore, the searching process is stopped when the objective function reaches a specific value related to the noise measurement in the input data. A brief flowchart of the solution method is presented in Figure 7.

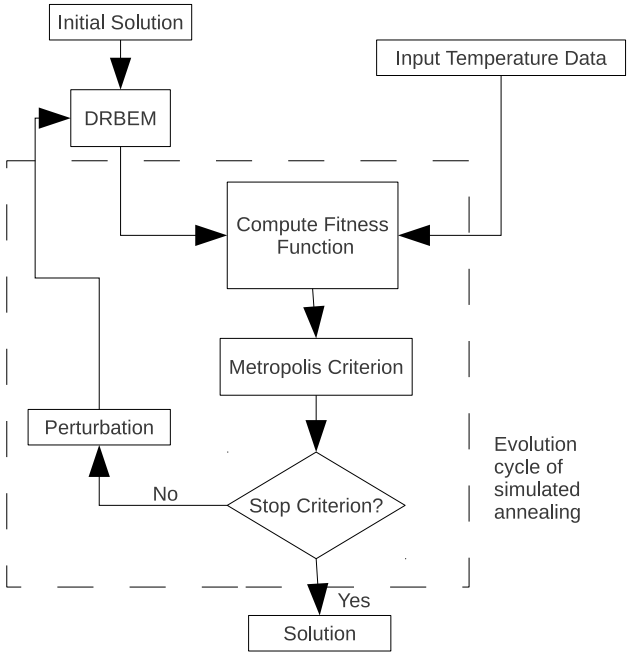

Figure 7. The inverse procedure based on simulated annealing.

Result

Results considering constant tumor size. In this section the results obtained for three tumors with constant size ($w \times d$=2 × 2 mm) and different blood perfusion rates are presented. The estimates for the tumor thickness and blood perfusion rate are presented in Table 3. For each level of noise the inverse process was carried out twice with different random initial solutions in order to test the robustness of the computation. In Case I, the exact blood perfusion is 0.0069$\text{ml}_\text{b}/\text{s.ml}_\text{t}$, that is 8 times higher than the perfusion in normal skin, and the maximum surface temperature difference is 0.132 °C. In order to show the influence of using an inappropriate number

of perturbations at each annealing temperature during the inverse process, results reported for this case were computed by considering 10 perturbations in the inverse process for the five levels of noise considered. The methodology works well considering noise with standard deviation less than 0.0123; however, by increasing the level of noise the results become less accurate if the number of perturbations is maintained constant. These results suggest that the number of perturbations in the minimization technique should be modified for the success of the searching process. In Case II the blood perfusion is 0.0047 $ml_b/s.ml_b$ (5.5 times higher than the perfusion in normal skin), which leads to an exact maximum difference in the surface temperature profile of 0.088 °C. It is clear that it is possible to estimate the tumor properties with good accuracy once appropriated parameters are used in the optimization technique. In this case the number of perturbations per annealing temperature was set at 25. In Case III the exact maximum difference in the surface temperature profile is 0.044 °C, which is smaller than those obtained in Cases I and II as the blood perfusion rate has been decreased to 3 times the perfusion in normal skin (0.0026 $ml_b/s.ml_t$ and). Again, results show good agreement between actual and predicted parameters regardless of the initial solution by taking into account 25 perturbations in the inverse process.

Results considering constant blood perfusion rate. In this section the results obtained for three tumors with constant blood perfusion (ω_b=4.7×10^{-3} $ml_b/s.ml_t$) and different invasion levels are presented. *Clark level II* (w×d=0.5 ×0.75 mm): in the experiments performed for this case, the result produced by the inverse process was a tumor measuring 0.7554 and 0.7868 mm thick with a blood perfusion of 4.8014×10^{-3} and 4.5172×10^{-3} $ml_b/s.ml_t$ respectively. The exact maximum difference in the surface temperature profile is 0.0456 °C. *Clark level III* (w×d=0.5×0.75 mm): the result produced by the methodology was for a tumor that is 1.0257, 0.9644 and 0.9464 mm thick, blood perfusion of 4.5621×10^{-3}, 4.5618×10^{-3} and 4.6372×10^{-3} $ml_b/s.ml_t$, respectively. The maximum noise standard deviation for this case was 2.2%. Figures 8 and 9 show the input surface temperature data for each level of noise considered in these cases, as well as the computed temperature profiles using the parameters predicted by the inverse process. *Clark level IV* (w×d=1.5×2.0 mm): considering as input data for the temperature distribution at the skin surface the values listed in Figure 10, the result produced by the inverse process was for a tumor that is 2.0084, 2.0252, 1.9989 and 2.0359 mm thick, with a blood perfusion 4.6835×10^{-3}, 4.7945×10^{-3}, 4.7033×10^{-3} and 4.2918×10^{-3} $ml_b/s.ml_t$, respectively.

Evolution of the estimation technique. This section discusses the evolution and convergence of the estimation technique. According to Figure 11, the initial guess did not affect the final estimate, indicating that the objective function has the global minimum in the region of interest. In this graphs, each marker represents the set of values accepted by simulated annealing during the minimization process. It is evident that the number of partial solutions accepted before the convergence, as well as the number of iterations, varies significantly for different levels of noise, as well as for each experiment. As the initial solutions are generated randomly, the predicted values for the thickness and blood perfusion are significantly inaccurate at the beginning of the process; however, there is a significant improvement as the number of perturbations increases (decrease of the annealing temperature). For the cases in Figures 11(a) and 11(b), all the experiments converged in almost the same number of iterations (2069). However, the number of solutions accepted was 12 for experiment 1, 4 for experiment 2, and 11 solutions for experiment 3. For all the cases presented, the behavior in the diversity of the number of iterations and solutions accepted prior to convergence prevails. This behavior is explained by the random nature of simulated annealing in proposing solutions. In some other cases, the searching process found the expected value immediately, and it was maintained constant

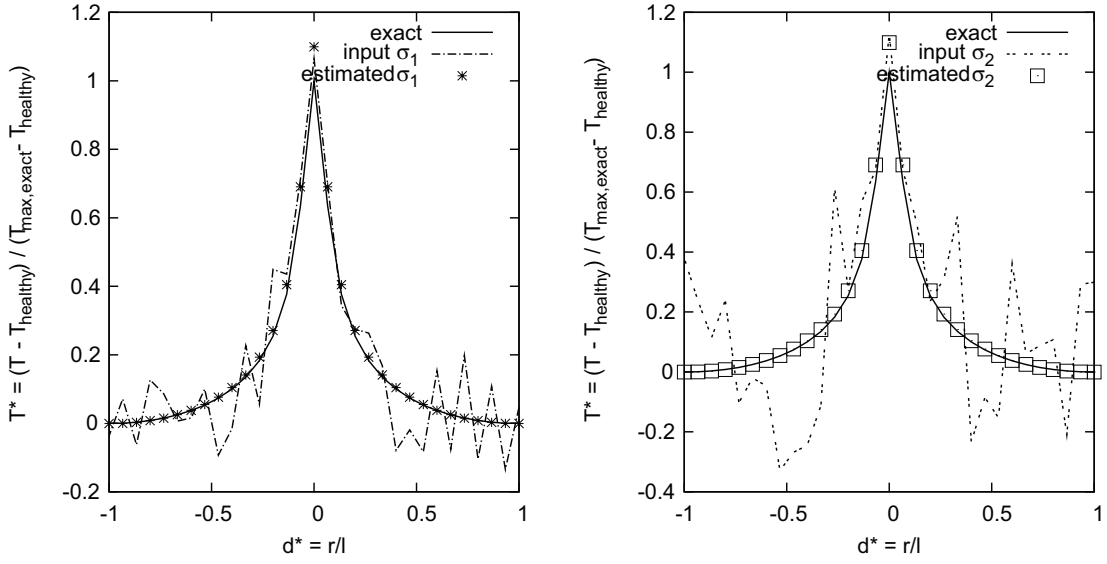

Figure 8. Exact, input and predicted surface temperature profiles for a tumor with a size w × d=0.5×0.75 mm, σ_1=0.46%, and σ_2=1.0% .

Table 3. Parameter estimates for Case I, Case II, and Case III.

Test	Exact Case I				Exact Case II				Exact Case III			
	2.0 (mm)		6.9×10^{-3} ($ml_b/s.ml_t$)		2.0 (mm)		4.7×10^{-3} ($ml_b/s.ml_t$)		2.0 (mm)		2.6×10^{-3} ($ml_b/s.ml_t$)	
	Estimated		% Error		Estimated		% Error		Estimated		% Error	
	d (mm)	$\omega_b\times10^{-3}$ ($ml_b/s.ml_t$)	d	ω_b	d (mm)	$\omega_b\times10^{-3}$ ($ml_b/s.ml_t$)	d	ω_b	d (mm)	$\omega_b\times10^{-3}$ ($ml_b/s.ml_t$)	d	ω_b
	σ_1=0.58%				σ_1=0.56%				σ_1=0.56%			
1	2.0216	6.8048	1.1	1.4	1.9883	4.7056	0.6	0.1	2.0027	2.5502	0.1	1.9
2	2.0064	6.8358	0.3	0.9	1.9838	4.6971	0.8	0.1	1.9778	2.5959	1.2	0.2
	σ_1=1.2%				σ_1=0.94%				σ_1=0.94%			
1	2.0366	6.7435	1.8	2.3	2.0432	4.6060	2.2	2.0	1.9758	2.5590	1.2	1.6
2	2.0459	6.7124	2.3	2.7	1.9750	4.8507	1.3	3.2	2.0162	2.6874	0.8	3.4
	σ_1=1.6%				σ_1=1.6%				σ_1=1.6%			
1	1.9021	7.2146	4.9	4.5	1.8932	4.9353	5.3	5.0	1.9682	2.5026	1.6	3.7
2	1.9026	7.3248	4.9	6.2	2.0213	4.6173	1.1	1.8	1.9839	2.5994	0.8	0.02
	σ_1=2.2%				σ_1=2.2%				σ_1=2.2%			
1	2.2044	6.1969	10.2	10.2	1.9559	4.8965	2.2	4.2	1.9773	2.7592	1.1	6.1
2	2.2534	6.0430	12.6	12.4	1.9682	4.8452	1.6	3.1	2.0074	2.7139	0.4	4.4
	σ_1=3.0%				σ_1=3.0%				σ_1=3.0%			
1	1.6795	8.5	16	23.2	1.9565	4.7673	2.2	1.4	1.9119	2.6687	4.4	2.6
2	1.7820	8.3247	10.9	20.6	1.9839	4.6907	0.8	0.2	2.0441	2.5576	2.2	1.6

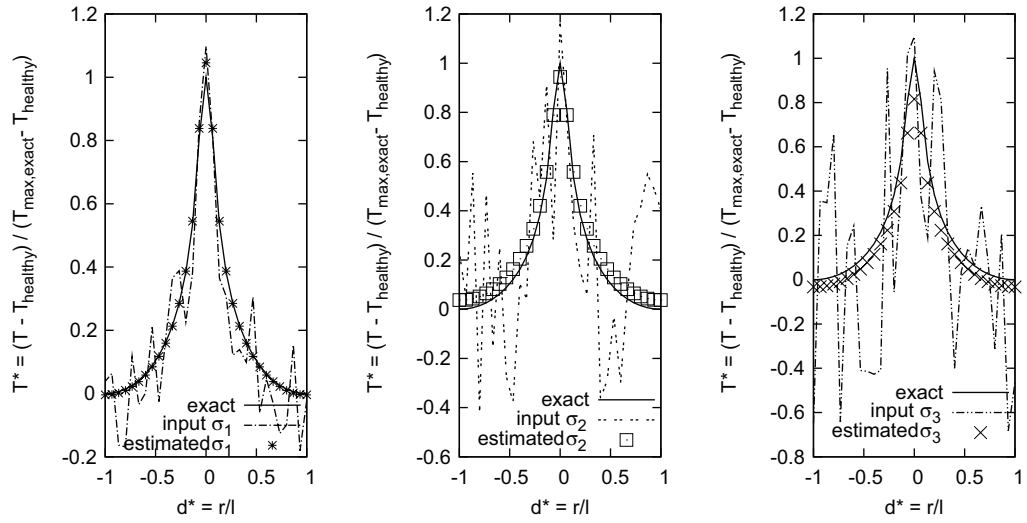

Figure 9. Exact, input and predicted surface temperature profiles for a tumor with a size $w \times d$=0.8×1.0 mm, σ_1=0.6%, σ_2=1.8% and σ_3=2.2%.

throughout the rest of the process, such as in the searching of the thickness in Figure 11(d) for different levels of noise.

Conclusions

Based on the accuracy of the results obtained for the hypothetical cases studied here, it was found that the inverse method works satisfactorily in the simultaneous estimation of unknown parameters under the consideration of extremely small surface temperature gradients, even in the case when noise was added to the input data. In general terms, the results show excellent agreement between the exact and predicted parameters, with an absolute error in the estimation of the thickness within 5.4% and an absolute error in the estimation of the blood perfusion within 9.5%.

Although the inverse process has focused on bio-heat transfer problems to evaluate geometric and thermophysical parameter of possible malignant cancerous regions in the human skin, several aspects of this research merit further investigation in order to be used in realistic clinical situations. For example, the methodology presented here requires dealing with temperature-dependent thermo-physical properties, which are particularly relevant when considering hyperthermia cancer therapy, as well as 3D cases to study the ability of the procedure to detect arbitrarily embedded tumor and geometries, such as would be found in clinical trials. The potential of the DRBEM and simulated annealing in adequately detecting geometrical and thermo-physical properties of vascularized, non-uniform skin tumors will significantly impact the applicability of this approach as a valuable clinical tool.

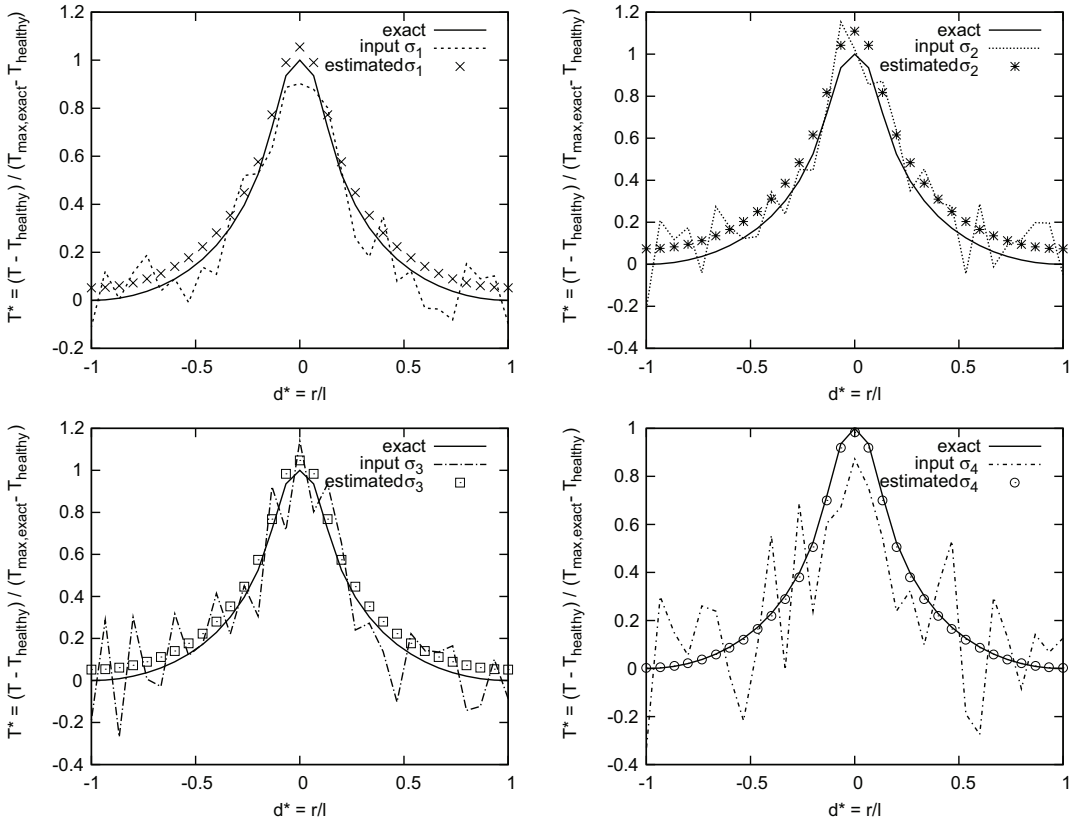

Figure 10. Exact, input and predicted surface temperature profiles for a tumor with a size $w \times d$=1.5×2.0 mm, σ_1=1.2%, σ_2=1.5%, σ_3=2.1% and σ_4=2.9%.

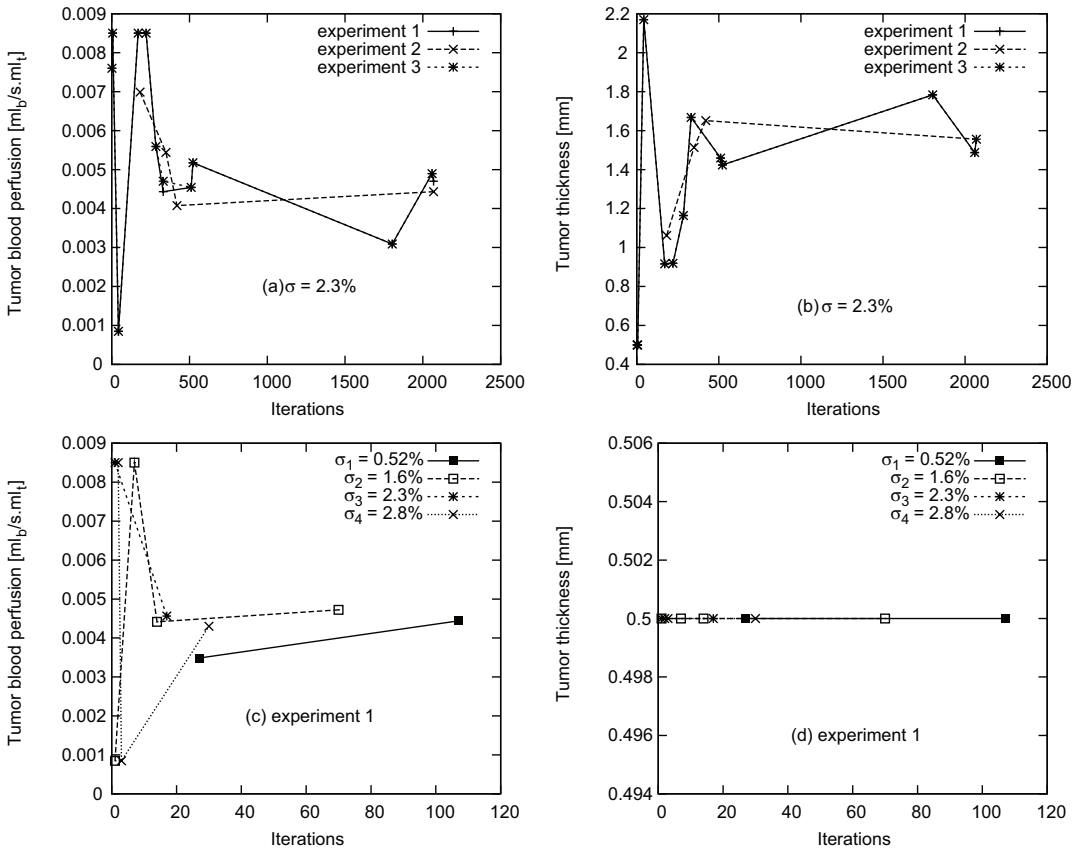

Figure 11. Convergence of the inverse process.

References

[1] Riegel, D.S. Carucci, J.A. *Malignant melanoma: prevention, early detection and treatment in the 21st century*, A Cancer Journal of Clinicians 50(2000) 215-236.

[2] Clark, W.H. From, L. Bernadino, E.A. Mihm, M.C. *The histogenesis and biologic behavior of primary human malignant melanomas of the skin*, Cancer Research 59(1969) 705-726.

[3] Breslow, A. Thikness, *cross-sectional area, and depth of invasion in the prognosis of cutaneous melanoma*, Annals of Surgery 172(1970) 902-908.

[4] Warburg, O. *Metabolism of Tumours*, Constable & Co, London, 1930.

[5] Brasfield, R.D. Laughlin, J.S. Sherman, R.S. *Thermography in the management of cancer* Annals of the N.Y. Academy of Sciences 121(1964) 235-247.

[6] Cetingul, M.P. Herman, C. *Quantification of the thermal signature of a melanoma lesion*, International Journal of Thermal Sciences 50(2011) 421-431.

[7] Santa Cruz, G.A. Bertotti, J. Marin, J. Gonzalez, S.J. Gossio, S. Alvarez, D. Roth, B.M.C. Menendez, P. Pereira, M.D. Albero, M. Cubau, L. Orellano, P. Liberman, S.J. *Dynamic infrared imaging of cutaneous melanoma and normal skin in patients treated with BNCT*, Applied Radiation and Isotopes 67(2009) S54-S58.

[8] Keyserlingk, J. Ahlgren, P. Yu, E. Belliveau, N. Yassa, M. *Functional infrared imaging of the breast*, IEEE Engineering in Medicine and Biology Magazine 19(2000) 30-41.

[9] Paruch, M. Majchrzak, E. *Identification of tumor region parameters using evolutionary algorithm and multiple reciprocity boundary element method*, Engineering Applications of Artificial Intelligence 20(2007) 647-655.

[10] Partridge, P.W. Wrobel, L.C. *An inverse geometry problem for the localization of skin tumours by thermal analysis*, Engineering Analysis with Boundary Elements 31(2007) 803-811.

[11] Mital, M. Scott, E.P. *Thermal detection of embedded tumors using infrared imaging*, ASME Journal of Biomechanical Engineering 129(2007) 33-39.

[12] Agnelli, J.P. Barrea, A.A. Turner, C.V. *Tumor location and parameter estimation by thermography*, Mathematical and Computer Modelling 53(2011) 1527-1534.

[13] Luna, J.M. Romero-Mendez, R. Hernandez-Guerrero, A. Elizalde-Blancas, F. *Procedure to estimate thermophysical and geometrical parameters of embedded cancerous lesions using thermography,* ASME Journal of Biomechanical Engineering 134(2012) 03100781-89.

[14] Cetingul, M.P. Herman, C. *A heat transfer model of skin tissue for the detection of lesions: sensitive analysis*, Physics in Medicine and Biology 55(2010) 5933-5951.

[15] Liu, J. Xu, X. *Boundary information based diagnostics on the thermal states of biological bodies*, International Journal of Heat and Mass Transfer 43(2000) 2827-2839.

[16] Cooper, T.E. Trezek, G.J. *Correlation for thermal properties of some human tissues with water content*, Aerospace Medicine 42(1971) 24-28.

[17] Stucker, M. Horstmann, I. Nuchel, C. Rochling, A. Homann, A. *Blood flow compared in benign melanocytic naevi, malignant melanomas and basal cell carcinomas*, Clinical and Experimental Dermatology 24(1999) 107-111.

[18] Vaupel, P. Kallinowski, F. Okunie, P. *Blood flow, oxygen, nutrient supply and metabolic microenvironment of human tumors: a review*, Cancer Research 49(1989) 6449-6465.

[19] Huckaba, C.E. Tam, H.S. Darling, R.C. Downey, J.A. *Prediction of dynamic temperature distribution in the human body*, AICHE Journal 21(1975) 1006-1012.

[20] Kallinowski, F. Schlenger, K.H. Runkel, S. Kloes, M. Stohrer, M. Okunie, P. Vaupel, P. *Blood flow, metabolism, cellular microenvironment and growth rate of human tumors xenografts*, Cancer Research 49(1989) 3759-3764.

[21] Sien, H.P. Jain, R.K. *Temperature distributions in normal and neoplastic tissues during hyperthermia: lumped parameter analysis*, Journal of Thermal Biology 4(1979) 157-164.

[22] Duck, F.A. *Physical Properties of Tissue: A Comprehensive Reference Book*, Academic, New York, 1990.

[23] Torvi, D.A. Dale, J.D. *A finite element model of skin subjected to a flash fire*, ASME Journal of Biomechanical Engineering 116(1994) 250-255.

[24] Pennes, H.H. *Analysis of tissue and arterial temperatures in the resting human forearm*, Journal of Applied Physiology 1(1948) 93-122.

[25] Shih, T.C. Kou, H.S. Liauh, C.T. Lin, W.L. *Thermal models of bio-heat transfer equations in living tissue and thermal dose equivalence due to hyperthermia*, Biomedical Engineering – Applications, Basis & Communications 14(2002) 86-96.

[26] Fogelson, I.B. Berdkinov, S.I. Zavitkov, Y.V. *Electrical thermometers and sensors for measuring human body temperature*, Biomedical Engineering 30(1996) 211-213.

[27] Kirkpatrick S. Gelatt C.D. Vecchi M.P. *Optimization by Simulated Annealing*, Science, 220(1983) 671–680.

[28] Metropolis, N. Rosenbluth, A. Rosenbluth, M. Teller, A. Teller, E. *Equation of State Calculations by Fast Computing Machines*, Journal of Chemical Physics, 21(1953) 1087–1092.

[29] Ledesma, S. Avina, G. Sanchez, R. *Practical Considerations for Simulated Annealing Implementation*, Simulated Annealing (2008) 401-420.